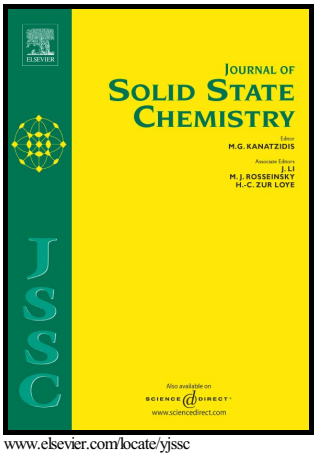

www.elsevier.com/locate/yjssc

W_3CoB_3-type {Y, Gd - Ho}$_3Co_{4-x}Al_x$ (x = 0.5 − 1) rare earth compounds: specific features of crystal structure and magnetic ordering

A.V. Morozkin, A.V. Garshev, A.V. Knotko, V.O. Yapaskurt, O. Isnard, Jinlei Yao, R. Nirmala, S. Quezado, S.K. Malik

PII: S0022-4596(17)30120-2
DOI: http://dx.doi.org/10.1016/j.jssc.2017.04.009
Reference: YJSSC19742

To appear in: *Journal of Solid State Chemistry*

Received date: 13 February 2017
Revised date: 13 March 2017
Accepted date: 8 April 2017

Cite this article as: A.V. Morozkin, A.V. Garshev, A.V. Knotko, V.O. Yapaskurt, O. Isnard, Jinlei Yao, R. Nirmala, S. Quezado and S.K. Malik, W_3CoB_3-type {Y, Gd - Ho}$_3Co_{4-x}Al_x$ (x = 0.5 − 1) rare earth compounds: specific features of crystal structure and magnetic ordering, *Journal of Solid State Chemistry,* http://dx.doi.org/10.1016/j.jssc.2017.04.009

W_3CoB_3-type {Y, Gd - Ho}$_3Co_{4-x}Al_x$ (x = 0.5 - 1) rare earth compounds: specific features of crystal structure and magnetic ordering

A. V. Morozkin [a*], A.V. Garshev [a, b], A.V. Knotko [a, b], V.O. Yapaskurt [c], O. Isnard [d, e], Jinlei Yao [f], R. Nirmala [g], S. Quezado [h], S.K. Malik [h]

[a] *Department of Chemistry, Moscow State University, Leninskie Gory, House 1, Building 3, Moscow, GSP-2, 119992, Russia*

[b] *Faculty of Materials Science, Moscow State University, Leninskie Gory, House 1, Building 73, Moscow, GSP-1, 119991, Russia*

[c] *Department of Petrology, Geological Faculty Moscow State University, Leninskie Gory, Moscow, 119992, Russia*

[d] *CNRS, Insitut. Néel, 25 rue des Martyrs BP166 x F-38042 Grenoble, France*

[e] *Université Grenoble Alpes, Inst. Néel, F-38042 Grenoble, France*

[f] *Jiangsu Key Laboratory of Micro and Nano Heat Fluid Flow Technology and Energy Application, School of Mathematics and Physics, Suzhou University of Science and Technology, Suzhou 215009, China*

[g] *Indian Institute of Technology Madras, Chennai 600 036, India*

[h] *Departamento de Física Teórica e Experimental, Universidade Federal do Rio Grande do Norte, Natal,59082-970, Brazil*

[*] *Corresponding author: morozkin@tech.chem.msu.ru*

Abstract

The crystal structure of new W_3CoB_3-type {Y, Gd - Ho}$_3Co_{3.25}Al_{0.75}$, $Gd_3Co_{3.5}Al_{0.5}$ and Tb_3Co_3Al compounds (*Cmcm*. N 63, *oC*28) has been established using powder X-ray diffraction studies. The magnetic properties of $Gd_3Co_{3.5}Al_{0.5}$, $Gd_3Co_{3.25}Al_{0.75}$ and $Tb_3Co_{3.25}Al_{0.75}$ were determined by bulk magnetization measurements and neutron diffraction studies. $Gd_3Co_{0.5}Al_{0.5}$, $Gd_3Co_{3.25}Al_{0.75}$ and $Tb_3Co_{3.25}Al_{0.75}$ exhibit ferrimagnetic ordering below 196 K, 161 K and 151 K, respectively.

$Tb_3Co_{3.25}Al_{0.75}$ shows a spin-reorientation transition at ~42 K. Below the ferrimagnetic ordering temperature $Gd_3Co_{3.25}Al_{0.75}$ and $Tb_3Co_{3.25}Al_{0.75}$ are soft ferrimagnets, meanwhile $Tb_3Co_{3.25}Al_{0.75}$ shows magnetic hardness below the spin-reorientation transition with remanent magnetization per formula unit of 9.7 μ_B and coercive field of 15 kOe at 2 K.

The magnetocaloric effects of $Gd_3Co_{3.25}Al_{0.75}$ and $Tb_3Co_{3.25}Al_{0.75}$ were calculated in terms of isothermal magnetic entropy change and they reach maximum values of -4.9 J/kg·K at 135-145 K and -3.7 J/kg·K at 115-135 K, respectively, for a field change of 0-50 kOe. Low temperature magnetic ordering in $Tb_3Co_{3.25}Al_{0.75}$ is accompanied by a positive magnetocaloric effect with isothermal magnetic entropy changes of +13.6 J/kg·K at 10 K for a field change of 0-50 kOe and +0.9 J/kg·K at 45 K for a field change of 0-10 kOe.

Neutron diffraction study in zero applied field shows mixed ferro-antiferromagnetic ordering of $Tb_3Co_{3.25}Al_{0.75}$ with a wave vector $\mathbf{K}_0$ = [0, 0, 0]. Below ~ 137 K $Tb_3Co_{3.25}Al_{0.75}$ exhibits non-collinear ferrimagnetic ordering of terbium and cobalt sublattices with resulting of *b*-axis ferromagnetic and *c*-axis antiferromagnetic components of **Cmc′m** = {**1**, $\mathbf{m}_x$} × {**1**, $\mathbf{m}_z$/[0, 0, 1/2]} × {**1**, **i′**} × {**1**, **1**/[1/2, 1/2, 0]} magnetic space group. The spin-reorientation transition in $Tb_3Co_{3.25}Al_{0.75}$ below ~38 K corresponds to appearance of additional *a*-axis ferromagnetic component and decreasing of symmetry of magnetic ordering down to **C2′/c** = {**1**, $\mathbf{m}_z$/[0, 0, 1/2]} × {**1**, **i′**} × {**1**, **1**/[1/2, 1/2, 0]} magnetic space group.

Key words: Rare earth compounds; Magnetic properties; Magnetocaloric effect; Neutron diffraction; Magnetic structure

1. Introduction

Intermetallic compounds composed of rare earth, transition metal and *p*-elements are being actively studied for the occurrence of large magnetocaloric effect over suitable temperature ranges for

applications in magnetic refrigeration/heating technologies and for the occurrence of giant coercive force as potential basis for permanent magnets.

The R_3Ge_4 (R = Rare earth) compounds displayed an intricate canted antiferromagnetic structure with two inequivalent sites for rare earth [1-2]. In particular, the Er_3Ge_4 compound undergoes an antiferromagnetic transition and a spin-reorientation transition and the entropy involved in spin-reorientation transition has been found to be larger in the earlier calorimetric studies [2]. Transition metal (Co, Fe, etc) substitution at the *p*-element site yielded interesting structural and magnetic properties [3-6]. Novel rare earth intermetallic compounds $\{Y, Gd - Ho\}_3Co_{4-x}Al_x$ ($x = 0.5$-1) crystallize in the W_3CoB_3-type structure (the ordered variant of Er_3Ge_4-type structure), such as Er_3FeGe_3 [3], $Gd_3Co_{2.48}Si_{1.52}$ [4], $\{Y, Gd, Dy - Tm\}_3Co_{2.2}Si_{1.8}$ [5] and $\{Y, Pr, Nd, Sm, Gd, Tb\}_3Co_3Ga$ [6]. These compounds belong to a large family of the two-layer orthorhombic structures with the *Cmcm* space group symmetry [5]. The structure is derived from the Mg-type rare earths via orthorhombic distortion of the initial hexagonal rare-earth lattice with the insertion of transition metals and *p* elements.

Till now the magnetic properties of Er_3FeGe_3 [3] and $\{Y, Pr, Nd, Sm, Gd, Tb\}_3Co_3Ga$ [6] were not investigated, whereas $Gd_3Co_{2.48}Si_{1.52}$ [4] and $\{Y, Gd, Dy - Tm\}_3Co_{2.2}Si_{1.8}$ [5] exhibit complex ferro-antiferromagnetic ordering: $Gd_3Co_{2.2}Si_{1.8}$ behaves as soft ferrimagnetic below Curie point [7], whereas $\{Tb, Dy\}_3Co_{2.2}Si_{1.8}$ are soft ferrimagnets below Curie points and they exhibit hard magnetic properties below the spin-reorientation temperature [8]. Neutron diffraction study in zero applied field indicates mixed ferro-antiferromagnetic of $Tb_3Co_{2.2}Si_{1.8}$ with wave vectors $\mathbf{K}_0 = [0, 0, 0]$ and $\mathbf{K}_1 = [\pm K_x, 0, 0]$ ($K_x \approx 3/10$): below $T_C = 125$ K the magnetic structure of $Tb_3Co_{2.2}Si_{1.8}$ is a set of canted ferromagnetic cones with a resulting *b*-axis ferromagnetic component and below $T_{SR} = 42$ K its magnetic structure is a set of canted ferromagnetic cones with a resulting *c*-axis ferromagnetic component (between 53 K and 42 K the high-temperature magnetic order of $Tb_3Co_{2.2}Si_{1.8}$ transforms to the low-temperature order via an intermediate state) [8].

This work reports the crystal structure of {Y, Gd - Ho}$_3$Co$_{4-x}$Al$_x$ (x =0.5-1) compounds, magnetic properties of $Gd_3Co_{3.5}Al_{0.5}$, $Gd_3Co_{3.25}Al_{0.75}$ and $Tb_3Co_{3.25}Al_{0.75}$ compounds and magnetic structure of $Tb_3Co_{3.25}Al_{0.75}$ from neutron diffraction study in zero applied field.

2. Experimental details

The {Y, Gd - Ho}$_3$Co$_{4-x}$Al$_x$ (x = 0.5-1) alloys were prepared by arc-melting the weighed amounts of rare earth (99.9 wt. %), Co and Al (99.95 wt. %). The samples were annealed at 870 K for 820 h in an argon atmosphere and subsequently quenched in ice-cold water. The quality of the samples was evaluated using powder X-ray diffraction and microprobe analyses. The X-ray data were obtained on a Rigaku D/MAX-2500 diffractometers (Cu K_α radiation, 2θ = 10-80 deg, step 0.02). An INCA-Energy-350 X-ray EDS spectrometer (Oxford Instruments) on the Jeol JSM-6480LV scanning electron microscope (20 kV accelerating voltage, beam current 0.7 nA and beam diameter 50 micron) was employed to perform the microprobe analysis of the sample. Signals averaged over three points per phase estimated standard deviations of 1 at. % for rare earth (measured by L-series lines), 1 at. % for cobalt and aluminium (measured by K-series lines).

Magnetization measurements on bulk polycrystalline piece of $Gd_3Co_{3.5}Al_{0.5}$, $Gd_3Co_{3.25}Al_{0.75}$ and $Tb_3Co_{3.25}Al_{0.75}$ samples were carried out using a vibrating sample magnetometer (VSM attachment on PPMS Dynacool System, Quantum Design, USA) in the temperature range of 2-300 K and in magnetic fields up to 140 kOe. Low field (100 Oe) magnetization data were obtained in zero-field-cooled (zfc) and field-cooled (fc) states to determine the magnetic ordering temperatures. The Curie temperature (T_C) was defined as the dM/dT minima and Neel (spin-reorientation) temperature (T_{SR}) was defined as M maximum of the thermal magnetization curve. Magnetization as a function of temperature was measured in 5 kOe field in zero-field-cooled state to obtain effective paramagnetic moment and paramagnetic Weiss temperature. Magnetization vs field hysteresis curves were recorded at different temperatures to obtain magnetization in field of 140 kOe (M_{140kOe}), remanent magnetization (M_{res}),

critical (H_{crit}) and coercive fields (H_{coer}). Magnetization isotherms were obtained at various temperatures ranging with a temperature step of 5 K (7 K) and a field step of 2.5 kOe to calculate isothermal magnetic entropy changes (ΔS_m).

Neutron diffraction experiments were carried out at the high flux reactor of the Institut Laue Langevin. (Grenoble, France) using the high flux powder diffractometer D1B operated by the CNRS-CRG team [9]. The diffraction patterns were recorded at several temperatures ranging from 140 K down to 1.5 K. The two axis D1B powder diffractometer used for this work is equipped with a large 1280 cells curved detector which records the diffraction pattern over a 2θ range of 130° with a 2θ step of 0.1°. The neutron wavelength of 0.252 nm was selected by the (002) reflection of a pyrolitic graphite monochromator.

3. Theory and calculations

The unit cell data were derived from powder XRD using the Rietan-program [10, 11] in the isotropic approximation at room temperature. Bilbao Crystallographic server [12] was used for analysis of W_3CoB_3-type structure [13] according to the symmetry tables of the International Tables of crystallography [14]. The paramagnetic susceptibility was fitted to the Curie-Weiss law and the effective magnetic moments and paramagnetic Weiss temperatures were obtained [15]. Magnetic field (H), coercive field (H_{coer}) and critical field (H_{crit}) are given in Oe unit (1 Oe = $10^3/4\pi$ A/m and magnetic field of 1 Oe corresponds to the strength of a magnetic field of 10^{-4} T). Magnetization is given in emu/g and μ_B units (1 emu/g = 1 A·m^2/kg, 1 μ_B = 9.7400968(20)·10^{-24} A·m^2) [15].

Magnetocaloric effect (MCE) is calculated in terms of the isothermal magnetic entropy change, ΔS_m, using the magnetization vs field data obtained near the magnetic transition using the thermodynamic Maxwell relation [16]. The neutron diffraction patterns were identified and calculated

using the Rietveld refinement method implemented in the FULLPROF-program [17]. The magnetic space groups [18] were used for the analysis of neutron diffraction patterns.

4. Results

4.1. Crystal structure

The X-ray powder analysis showed that the {Y, Gd - Ho}$_3$Co$_{3.25}$Al$_{0.75}$ ('$R_{43(1)}$Co$_{46(1)}$Al$_{11(1)}$' phases from microprobe analysis), Gd$_3$Co$_{3.5}$Al$_{0.5}$ ('Gd$_{44(1)}$Co$_{50(1)}$Al$_{7(1)}$' phase) and Tb$_3$Co$_3$Al ('Tb$_{43(1)}$Co$_{43(1)}$Al$_{14(1)}$' phase) crystallize in the W$_3$CoB$_3$-type structure (space group *Cmcm*, N 63, *oC*28) (**Figure 1s**). The refined unit cell data and atomic positions are given in **Table 1**. The shortest interatomic distances are close to the sum of metallic radii of corresponding atoms [19, 20] as shown for Tb$_3$Co$_{3.25}$Al$_{0.75}$ in **Table 2**.

We suggest that R_3Co$_{3.25}$Al$_{0.75}$ compounds exhibit phase homogeneity of R_3Co$_{4-x}$Al$_x$ (x = 0.5-1) in the *R*-Co-Al systems as Gd$_3$Co$_{3.5}$Al$_{0.5}$ and Tb$_3$Co$_3$Al were detected. Within this homogeneous area R_3Co$_{4-x}$Al$_x$ exhibit anisotropic distortion of unit cell vs cobalt (aluminum) content: from Gd$_3$Co$_{3.5}$Al$_{0.5}$ to Gd$_3$Co$_{3.25}$Al$_{0.75}$ cell parameter *a* increases, cell parameter *c* is close to constant, whereas cell parameter *b* and unit cell volume *V* decrease; from Tb$_3$Co$_{3.25}$Al$_{0.75}$ to Tb$_3$Co$_3$Al cell parameter *a* and unit cell volume *V* increase and cell parameters *b* and *c* decrease (**Table 1**).

4.2. Magnetic transitions

In a field of 100 Oe, Gd$_3$Co$_{3.5}$Al$_{0.5}$, Gd$_{3.25}$Al$_{0.75}$ and Tb$_3$Co$_{3.25}$Al$_{0.75}$ exhibit ferrimagnetic transitions at 196 K, 161 K and 151 K, respectively (**Figure 1**). In contrast with Gd-containing compounds, Tb$_3$Co$_{3.25}$Al$_{0.75}$ show a smooth antiferromagnetic-like transition at ~42 K. The paramagnetic susceptibility of Gd$_3$Co$_{3.5}$Al$_{0.5}$, Gd$_3$Co$_{3.25}$Al$_{0.75}$ and Tb$_3$Co$_{3.25}$Al$_{0.75}$ follows the Curie-Weiss law in the temperature range of ~280 to 300 K, ~220 to 300 K and ~200 to 300 K, respectively. The fit to the Curie-Weiss law yields positive paramagnetic Weiss temperatures Θ_p = 198 K for Gd$_3$Co$_{3.5}$Al$_{0.5}$, Θ_p =

39 K for $Gd_3Co_{3.25}Al_{0.75}$ and Θ_p = 118 K for $Tb_3Co_{3.25}Al_{0.75}$, suggesting dominant ferromagnetic interactions (**Figure 2**). The effective moments per formula unit, M_{eff}/fu, are 14.1 μ_B for $Gd_3Co_{3.5}Al_{0.5}$, 14.0 μ_B for $Gd_3Co_{3.25}Al_{0.75}$ and 17.1 μ_B for $Tb_3Co_{3.25}Al_{0.75}$, respectively. This suggests that the effective magnetic moments per Co are 1.7 μ_B, 1.5 μ_B and 1.7 μ_B, respectively, assuming that Gd and Tb take the theoretical effective magnetic moment values of 7.94 μ_B and 9.72 μ_B, respectively [21]. These values are close to the theoretical cobalt effective magnetic moment of 1.715 μ_B [21].

4.3. Magnetization

The magnetization vs magnetic field data of $Gd_3Co_{3.25}Al_{0.75}$ and $Tb_3Co_{3.25}Al_{0.75}$ are plotted in **Figure 3**. $Gd_3Co_{3.25}Al_{0.75}$ is soft ferrimagnetic down to 2 K with zero residual magnetization and coercive field. At 2 K the magnetization per formula unit of $Gd_3Co_{3.25}Al_{0.75}$ in field of 140 kOe (M_{140kOe}/fu) reaches value of 19.8 μ_B (saturation magnetization per formula unit M_∞/fu $\rightarrow$ 20.8 μ_B at 1/H $\rightarrow$ 0) (**Figure 3a**). This value corresponds to magnetization per Gd of M_{140kOe}/Gd = 6.6 μ_B which is close to the theoretical Gd magnetic moment of 7 μ_B [21], suggesting collinear ferrimagnetic ordering of gadolinium magnetic sublattice in $Gd_3Co_{3.25}Al_{0.75}$ with insignificant influence of magnetic Co sublattice.

$Tb_3Co_{3.25}Al_{0.75}$ is soft ferrimagnetic below T_C = 151 K and down to the spin-reorientation temperature (T_{SR} ~ 42 K in 5 kOe field), e.g., magnetization of M_{140kOe}/fu = 15.2 μ_B with zero residual magnetization and coercivity at 100 K (**Figure 3b**). Below T_{SR} $Tb_3Co_{3.25}Al_{0.75}$ exhibits permanent magnet properties, such as magnetization of M_{140kOe}/fu = 18.2 μ_B, residual magnetization per formula unit (M_{res}/fu) of 9.1 μ_B, coercive field (H_{coer}) of 14 kOe and critical field (H_{crit}) of ~ 10 kOe at 30 K (at 30 K M_∞/fu $\rightarrow$ 21.5 μ_B) and M_{140kOe}/fu = 17.3 μ_B, M_{res}/fu = 9.7 μ_B, H_{coer} = 15 kOe and H_{crit} ~ 12 kOe at 2 K (M_∞/fu $\rightarrow$ 21.5 μ_B at 2 K) (**Figures 3c** and **3d**). The magnetization values in 140 kOe indicate non-collinear/incomplete ferrimagnetic ordering of $Tb_3Co_{3.25}Al_{0.75}$ below T_C.

4.4. Magnetocaloric effect (MCE)

The magnetocaloric effects of $Gd_3Co_{3.25}Al_{0.75}$ and $Tb_3Co_{3.25}Al_{0.75}$ were calculated in terms of the isothermal magnetic entropy change, ΔS_m, from the magnetization vs field data (**Figure 2s**).

The magnetocaloric effect of $Gd_3Co_{3.25}Al_{0.75}$ around ~140 K corresponds to the paramagnetic to ferrimagnetic transition (T_C = 161 K): the magnetic entropy change, ΔS_m, reaches a value of -4.9 J/kg·K for a field change of 50 kOe at 135-145 K (**Figure 4a**) and a values of -11.3 J/kg·K for a field change of 140 kOe at 125 - 145 K (**Figure 3s-a**). The maximal magnetic entropy change, ΔS_m^{max}, at 140 K shows almost linear dependence vs field change (inserted in **Figure 4a**).

The magnetocaloric effect of $Tb_3Co_{3.25}Al_{0.75}$ (ΔS_m) reaches a value of -3.7 J/kg·K at 115-135 K and +13.6 J/kg·K at 10 K for a field change of 50 kOe (**Figure 4b**) and a value of -9.9 J/kg·K at 115-135 K and +32.9 J/kg·K at 5 K for a field change of 140 kOe (**Figure 3s-b**). The magnetocaloric effect at 115-135 K corresponds to the paramagnetic to ferrimagnetic transition of $Tb_3Co_{3.25}Al_{0.75}$ (T_C = 151 K), whereas low-temperature magnetocaloric effect corresponds to the field induced antiferromagnetic transition/spin reorientation or magnetocrystalline anisotropy in $Tb_3Co_{3.25}Al_{0.75}$. The maximum magnetic entropy change, ΔS_m^{max}, at 130 K shows almost linear dependence, whereas low-temperature ΔS_m^{max} shows saturated behaviour vs field change with shifting of maxima from 45 K (field change of 0-10 kOe) to 5 K (field change of 0-140 kOe) (inserted in **Figure 4b**).

The results of magnetization measurements of $Gd_3Co_{3.5}Al_{0.5}$, $Gd_3Co_{3.25}Al_{0.75}$ and $Tb_3Co_{3.25}Al_{0.75}$ are summarized in **Table 3**. The temperature of magnetic transitions of $Gd_3Co_{3.25}Al_{0.75}$ and $Tb_3Co_{3.25}Al_{0.75}$ does not follow de Gennes rule [21], indicating possible differences in their magnetic structures. If magnetic ordering of $Tb_3Co_{3.25}Al_{0.75}$, $Dy_3Co_{3.25}Al_{0.75}$ and $Ho_3Co_{3.25}Al_{0.75}$ follows de Gennes rule [21], $Dy_3Co_{3.25}Al_{0.75}$ and $Ho_3Co_{3.25}Al_{0.75}$ should exhibit ferromagnetic ordering at 100 K and 65 K and following spin-reorientation transition at 30 K and 20 K, respectively. The increasing of cobalt content in $\{Tb - Ho\}_3Co_{3.25}Al_{0.75}$ compounds up to $\{Tb, - Ho\}_3Co_{2.5}Al_{0.5}$ composition should lead to noticeable

increasing of their temperature of ferromagnetic ordering as the Curie temperature of $Gd_3Co_{3.5}Al_{0.5}$ (T_C = 196 K) is significantly bigger than the Curie temperature of $Gd_3Co_{3.25}Al_{0.75}$ (T_C = 161 K).

4.5. Neutron diffraction study of $Tb_3Co_{3.25}Al_{0.75}$

A priori, the magnetic ordering of $Tb_3Co_{3.25}Al_{0.75}$ may be result of magnetic ordering of Tb and Co in the corresponding atomic positions of unit cell and magnetic structure of $Tb_3Co_{3.25}Al_{0.75}$ may be viewed as a set of 4*c* and 8*f* magnetic terbium and cobalt sublattices with uncertain magnetic ordering of one Co atoms in the 4*a* site (M = $Co_{0.25}Al_{0.75}$) with uncertain position of Co atom in this site of unit cell (**Table 1**). For this reason, the only model with magnetic ordering of 4*c* and 8*f* magnetic terbium and cobalt sublattices was used for determination of $Tb_3Co_{3.25}Al_{0.75}$ magnetic structure.

The coordinates for the 4*c* and 8*f* sites and symmetry operators of these terbium and cobalt sublattices are given in **Table 4**.

Below T_C^{ND} ~137 K, the observed set of magnetic reflections reveals the magnetic ordering of $Tb_3Co_{3.25}Al_{0.75}$ with $\mathbf{K}_0$ = [0, 0, 0] wave vector (**Figure 5**). Thermal variation of structural and magnetic reflections indicates two types of magnetic ordering of $Tb_3Co_{3.25}Al_{0.75}$: between T_C^{ND} ~137 K and T_{SR}^{ND} ~ 38 K (high-temperature ordering HT) and below T_{SR}^{ND} ~ 38 K (low-temperature ordering LT) (**Figure 5d**). The high-temperature magnetic ordering at ~137 K (T_C^{ND}) corresponds to the Curie point of $Tb_3Co_{3.25}Al_{0.75}$, whereas transformation of magnetic scattering at ~38 K (T_{SR}^{ND}) corresponds to the magnetic transition obtained at ~42 K from magnetization measurement.

Analysis of neutron diffraction patterns (NDP) shows that the following variants of commensurate magnetic structure is in the best agreement with experiments:

- the Tb1 sublattice is divided for $Tb1^{1,3,5,7}$ and $Tb1^{2,4,6,8}$ sublattices with different orientation of magnetic moments; the Co1 sublattice is divided for $Co1^{1,3,5,7}$ and $Co1^{2,4,6,8}$ sublattices with different orientation of magnetic moments, whereas Tb2 ($Tb2^{1,2,3,4}$) and Co2 ($Co2^{1,2,3,4}$) sublattices show same magnetic ordering for terbium and cobalt atoms, respectively;

- the $Tb1^{1,3,5,7}$ and $Co1^{1,3,5,7}$, $Tb1^{2,4,6,8}$ and $Co1^{2,4,6,8}$, $Tb2^{1,2,3,4}$ and $Co2^{1,2,3,4}$ sublattices exhibit antiferromagnetic ordering;

- between ~137 K and 38 K the mixed *b*-axis ferromagnetic (ferrimagnetic) $\mathbf{F}_b = [\mathbf{F}_b(\text{Tb}) - \mathbf{F}_b(\text{Co})]$ and *c*-axis antiferromagnetic (anti-ferrimagnetic) $\mathbf{AF}_c = [\mathbf{AF}_c(\text{Tb}) - \mathbf{AF}_c(\text{Co})]$ ordering of **Cmc′m** = {**1**, $\mathbf{m}_x$} × {**1**, $\mathbf{m}_z$/[0, 0, 1/2]} × {**1**, **i′**} × {**1**, **1**/[1/2, 1/2, 0]} magnetic space group (N 63.4.514) [18]: $(\mathbf{F}_b + \mathbf{AF}_c)^{K0}$ **Cmc′m** (**Table 5** and **Figure 6a**);

- below 38 K the resulting mixed *ab*-axis ferromagnetic (ferrimagnetic) $(\mathbf{F}_a + \mathbf{F}_b) = [\mathbf{F}_a(\text{Tb}) - \mathbf{F}_a(\text{Co}) + \mathbf{F}_b(\text{Tb}) - \mathbf{F}_b(\text{Co})]$ and *c*-axis antiferromagnetic (anti-ferrimagnetic) $\mathbf{AF}_c = [\mathbf{AF}_c(\text{Tb}) - \mathbf{AF}_c(\text{Co})]$ ordering of **C2′/c** = {**1**, $\mathbf{m}_z$/[0, 0, 1/2]} × {**1**, **i′**} × {**1**, **1**/[1/2, 1/2, 0]} magnetic space group (N 15.3.94) [18]: $(\mathbf{F}_a + \mathbf{F}_b + \mathbf{AF}_c)^{K0}$ **C2′/c** (**Table 5** and **Figure 6b**).

Thermal variation of *a*-, *b*-, *c*-axis magnetic components and resulting magnetic moment of corresponding Tb1, Tb2, Co1 and Co2 atoms are given in **Figures 7a-d**. At 1.5 K the magnetic moments of terbium and cobalt reach values of $M_{Tb1} = 9.0\ \mu_B$, $M_{Tb2} = 8.5\ \mu_B$, $M_{Co1} = 0.62\ \mu_B$ and $M_{Co2} = 0.28\ \mu_B$ (**Table 5**). The magnitude of terbium magnetic moment is close to the theoretical Tb magnetic moment of 9 μ_B [21], whereas cobalt magnetic moment is less than the elemental cobalt magnetic moment of 1.7 μ_B [21]. The remarkably small Co atomic moments refined in $Tb_3Co_{3.25}Al_{0.75}$ can be explained by their peculiar local atomic environment. As was previously discussed elsewhere, the short Co-Al bounding plays in favor of a reduction of the Co magnetic moment magnitude as a result of the electronic shell hybridization with the metalloid. Such interpretation has been revealed by neutron diffraction upon substitution of Al for Co in RCo_5 compounds [22, 23] and later confirmed both experimentally by X-ray photoemission spectroscopy (XPS) and theoretically by electronic structure calculations [24, 25]. XPS measurements have shown that the hybridization between the rare-earth 5d6s and Al 3sp and 4sp states and Co 3d states leads to a partial filling of the Co 3d band and to a decrease of the Co magnetic moments in comparison with the value in pure Co metal. The Co1 position has an

average of 1.5 Al as nearest neighbours. For the Co2 position, the even smaller magnetic moment obtained in the $Tb_3Co_{3.25}Al_{0.75}$ originates from the Tb rich environment since seven out of the nine near neighbors are Tb ones. Indeed the *R*-Co bounds are known to promote the reduction of the Co magnetic moment by electronic effect on the Co 3d band, a feature already reported in *R*-Co binaries [26] where the Co magnetic moment can even vanish for the high *R* concentrations. The increasing of magnetic moments of Tb2, Co1 and Co2 sublattices at the spin-orientation transition indicates the crucial role of these magnetic sublattices in the low-temperature ordering of $Tb_3Co_{3.25}Al_{0.75}$.

The unit cell of $Tb_3Co_{3.25}Al_{0.75}$ undergoes anisotropic compression: below the ferromagnetic transition $\Delta a/a_{140K} \approx \Delta c/c_{140K} < \Delta b/b_{140K}$, below spin-reorientation transition (at 24 K) $\Delta a/a_{140K} < \Delta c/c_{140K} \approx \Delta b/b_{140K}$ and below 24 K the $\Delta a/a_{140K}$, $\Delta b/b_{140K}$, $\Delta c/c_{140K}$ and $\Delta V/V_{140K}$ relative parameters are close to constant (**Figure 7e**). At 1.5 K the $\Delta a/a_{140K}$, $\Delta b/b_{140K}$ and $\Delta c/c_{140K}$ reach the values of -0.00128, -0.00098 and -0.00096, respectively, whereas $\Delta V/V_{140K}$ = -0.00322. Such behavior of the lattice parameters is clearly related to magnetic ordering and indicates magnetovolume correlations.

5. Discussion

As shown in Bilbao Crystallographic Server [12], *Cmcm* space group may be given in *Pnma*, *Pmmn*, *Pnnm*, *Pnna*, *Pmma*, *Pbcm*, *Pbcn*, *Cmc*2_1, *Amm*2, *Ama*2, *C*222_1, *C*2/*c*, *C*2/*m* and *P*2_1/*m* maximal subgroups in different axis and *Cmcm* group may be viewed as a maximal subgroup of hexagonal *P*6_3/*mmc* group. The W_3CoB_3-type unit cell (type structure) [14, 27] may be given in term of *Pnma*, *Pbcn*, *Pbcm*, *Pnna*, *Ama*2, *C*222_1, *C*2/*c* and *P*2_1/*m* space groups corresponding to possible distortion of lattice and W_3CoB_3-type unit cell may be described in term of *Pnma*, *Pnnm*, *Pmmn*, *Pmma*, *Amm*2, *Cmc*2_1 and *C*2/*m* space groups with distortion and destruction of some initial sublattice on the two sublattices as shown in **Figure 4s**. These modifications of W_3CoB_3-type lattice may be observed in solid solution based on the $R_3T_{4-x}X_x$ compounds, they may be obtained at various synthesis conditions,

due to magnetic ordering of W_3CoB_3-type lattice or structural transformation of lattice and different temperatures. Meanwhile, from the known structural types, the $La_3Ni_2Ga_2$-type (*Pbcm*, N 57, *oP*28) [27], Gd_3NSe_3-type [28], $NdRh_2Sn_4$-type [27, 29] and Sm_2NiSn_4-type [27, 30] (*Pnma*, N 62, *oP*28), $Ce_3Pd_6Sb_5$-type (*Pmmn*, N 59, *oP*28) [27, 31], $Er_8Si_{17}B_3$-type ($Cmc2_1$, N 36, *oC*28) [27, 32] and Sc_3NiSi_3-type (*C*2/*m*, N 12-2, *mC*28) [27, 33] structures may be viewed as structural derivatives of initial W_3CoB_3-type structure [14, 27].

The replacing of Si for Al and Ga in the '$Tb_3Co_{2.2}Si_{1.8}$ [5, 8] - $Tb_3Co_{3.25}Al_{0.75}$ - Tb_3Co_3Ga [6]' row leads to anisotropic distortion of initial $Tb_3Co_{2.2}Si_{1.8}$ unit cell with increasing of *c* cell parameter and unit cell volume *V* and decreasing of *b* cell parameters, whereas *a* cell parameter is close to constant in this row (**Figure 8a**). The cell parameters in the '$R_3Co_{2.2}Si_{1.8}$ [5, 8] - $R_3Co_{3.25}Al_{0.75}$ - R_3Co_3Ga [6]' rows (*R* = Y, Gd, Dy-Ho) show same behavoiur (see **Table 1**).

The distortion of unit cell and changes in the Co sublattices from $Tb_3Co_{2.2}Si_{1.8}$ [5, 8] to $Tb_3Co_{3.25}Al_{0.75}$ determine the difference in their magnetic ordering (see **Tables 3** and **5**):

- in spite of expansion of unit cell, temperature of ferrimagnetic ordering of $Tb_3Co_{3.25}Al_{0.75}$ (T_C = 151 K) is larger than the Curie point of $Tb_3Co_{2.2}Si_{1.8}$ (T_C = 132 K [5]) due to increasing of Co content and change in Co sublattices;

- $Tb_3Co_{3.25}Al_{0.75}$ and $Tb_3Co_{2.2}Si_{1.8}$ [8] show similar high-temperature magnetic ordering: same ($\mathbf{F}_b$ + $\mathbf{AF}_c$)$^{\mathbf{K0}}$ **Cmc′m** commensurate component (in contrast to $Tb_3Co_{2.2}Si_{1.8}$, the magnetic ordering of Co sublattices suppresses the incommensurate antiferromagnetic component in $Tb_3Co_{3.25}Al_{0.75}$) with soft ferromagnetic properties;

- $Tb_3Co_{3.25}Al_{0.75}$ and $Tb_3Co_{2.2}Si_{1.8}$ show low-temperature spin-reorientation ordering with additional *a*-axis ferromagnetic component and low-temperature permanent magnet properties, but with different low-temperature magnetic structures.

The following expansion of unit cell from $Tb_3Co_{3.25}Al_{0.75}$ to Tb_3Co_3Ga may lead to decreasing of ferromagnetic interactions in Tb_3Co_3Ga, decreasing of temperature of ferrimagnetic ordering with

similar magnetic structure and magnetic ordering of Tb_3Co_3Ga and $Tb_3Co_{3.25}Al_{0.75}$: high-temperature soft ferromagnetic properties and low-temperature permanent magnet properties due to spin-reorientation transition.

The high-temperature ferrimagnetic-type ordering corresponds to the negative magnetic entropy change, whereas low-temperature spin-reorientation ordering (rotation of ferromagnetic component) determines positive ΔS_m value for polycrystalline $Tb_3Co_{3.25}Al_{0.75}$, namely.

Within homogeneity area the '$Gd_3Co_{3.5}Al_{0.5}$ - $Gd_3Co_{3.25}Al_{0.75}$' and '$Tb_3Co_{3.25}Al_{0.75}$ - Tb_3Co_3Al' compounds show slight anisotropic distortion of unit cell (**Figure 8b**). Thus, the change in Co sublattices from $Gd_3Co_{3.25}Al_{0.75}$ to $Gd_3Co_{3.5}Al_{0.5}$ is the main reason for increasing of Curie point from 161 K in $Gd_3Co_{3.25}Al_{0.75}$ up to 196 K in $Gd_3Co_{3.5}Al_{0.5}$: the set of isolated Co atom with uncertain position and with uncertain magnetic ordering in 4*a* M = $Co_{0.25}Al_{0.75}$ sublattice of $Gd_3Co_{3.25}Al_{0.75}$ transforms in to the additional magnetic Co sublattice in the M = $Co_{0.5}Al_{0.5}$ site of $Gd_3Co_{3.5}Al_{0.5}$.

Thus, the type of rare earth, transition metal and *p*-element sublattices determine the distortion level of W_3CoB_3-type lattice and magnetic ordering of $R_3Co_{4-x}Al_x$ (x = 0.5...1) compounds with magnetic rare earth and cobalt sublattices.

6. Conclusion

The {Y, Gd - Ho}$_3Co_{3.25}Al_{0.75}$, $Gd_3Co_{3.5}Al_{0.5}$ and Tb_3Co_3Al compounds supplement the series of W_3Co_3B-type rare earth compounds. They show ferrimagnetic ordering and they exhibit homogeneity area $R_3Co_{3...3.5}Al_{1...0.5}$ in corresponding ternary *R*-Co-Al system with transformation of magnetic Co sublattice and magnetic ordering. Large Tb magnetic moment close to the expected trivalent state is observed at low temperature in $Tb_3Co_{3.25}Al_{0.75}$ while small magnetic moment of Co is obtained on both cobalt positions as a result of the strong chemical bonds with the Al and Tb nearest neighbours.

Acknowledgments

This work is supported by *Russian Fund for Basic Research* through the project N° 16-03-00666-a and the National Natural Science Foundation of China (Grant No. 51301116), the 333 Project, the Six-Summit Project of Jiangsu (Grant No. 2013-XCL-038). SKM thanks CAPES, Brazil for the award of a fellowship. The Institute Laue Langevin is warmly acknowledged for the use of the neutron diffraction beamtime as well as the CRG-instruments. The unit cell data of $Gd_3Co_{3.5}Al_{0.5}$ used with permission - © JCPDS - International Centre for Diffraction Data. A.V. Garshev and A.V. Knotko acknowledge partial support from M.V.Lomonosov Moscow State University Program of Development. R. N thanks DST-RFBR for support.

References

[1] P. Schobinger-Papamantellos, O. Oleksyn, C. Ritter, C. H. de Groot, K. H. J. Bushcow, J. Magn. Magn. Mater. **169** (1997) 253–260.

[2] Y. Y. Chen, Y. D. Yao, Y. S. Lin, C. L. Chang, H. H. Hamdeh, J. C. Ho, Phys. Rev. B **61** (2000) 58.

[3] O.I. Bodak, O.Y. Oleksin, M.F. Fedyna, V.K. Pecharskii, Inorg. Mater. **28** (1992) 371–374.

[4] E. Gaudin, C. Mayer, F. Weill, B. Chevalier, J. Alloys Compd. 545 (2012) 148–152.

[5] A.V. Morozkin, J. Yao, Y. Mozharivskyj, J. Solid State Chem. **192** (2012) 371–376.

[6] Y.P. Yarmolyuk, Y. Grin, E.I. Gladyshevskii, Dopov. Akad. Nauk Ukr. RSR, Ser. A (1978) 855–858 (*In Russian*).

[7] J. Yao, A. V. Morozkin, Y. Mozharivskyj, J. Alloys Compd. 550 (2013) 331–334.

[8] A.V. Morozkin, O. Isnard, R. Nirmala, S.K. Malik, J. Magn. Magn. Mater. 389 (2015) 157–168

[9] www.ill.eu, Yellow Book

[10] F. Izumi, "The Rietveld Method," ed. by R.A. Young, Oxford University Press, Oxford (1993) 13.

[11] F. Izumi, The Rigaku Journal 6(1) (1989) 10-20.

[12] Bilbao Crystallographic Server [The crystallographic site at the Condensed Matter Physics Dept. of

the University of the Basque Country], http://www.crys.ehu.es.

[13] International Tables for crystallography vol. A (2016) , John Wiley and Sons Inc. New York, DOI: 10.1107/97809553602060000001.

[14] O.Ya. Oleksyn, O.I. Bodak, J. Alloys Compd. 210 (1994) 19–21.

[15] R.A. Levy. Principles of Solid State Physics, Academic Press, NY USA 1968.

[16] A.M. Tishin, Y.L. Spichkin, The Magnetocaloric Effect and Its Applications, Institute of Physics Publishing, Bristol, Philadelphia (2003) 480.

[17] J. Rodriguez-Carvajal, Physica B 192 (1993) 55-69.

[18] D. B. Litvin, Magnetic Group Tables, 1-, 2- and 3-Dimensional Magnetic Subperiodic Groups and Magnetic Space Groups,, International Union of Crystallography, 2013 ISBN 978-0-9553602-2-0 doi:10.1107/9780955360220001. Reviewed by the IUCr Commission on Magnetic Structures.

[19] J. Emsley, The elements. Second edition, Clarendon press – Oxford (1991).

[20] Fizicheskie velichiny (Physical Data). Handbook. Ed. by I.S.Grigor'ev, E.Z.Meilohov, Moscow, Energoatomizdat, 1994 (*In Russian*).

[21] S. Legvold, Rare Earth Metals and Alloys, Ferromagnetic Materials, Ed. by P.Wohlfarth, Amsterdam, North-Holland Publ. Co. (1980) 183–295.

[22] C. Zlotea, O. Isnard, J. Phys.: Condens. Matter. 14 (2002) 10211-10220.

[23] C. Zlotea, O. Isnard, J. Magn. Magn. Mater. 253 (2002) 118-129.

[24] A. Laslo, R. Dudric, M. Neumann, O. Isnard, M. Coldea, V. Pop, Solid State Commun. 199 (2014) 43-46.

[25] D. Benea, O. Isnard, N. Coroian, V. Pop, J. Magn. Magn. Matter. 322 (2010) 1052-1055.

[26] D. Gignoux, D. Schmitt, J. Magn. Magn. Matter. 100 (1991) 99-125.

[27] Springer Materials The Landolt-Börnstein Database - Materials Science Data for 250000 Substances, http://www.springermaterials.com.

[28] C. M. Schurz, P. Talmon-Gros, F. Lissner, T. Schleid, Solid State Sciences 17 (2013) 140-145.

[29] M. Meot-Meyer, G. Venturini, B. Malaman, B. Roques, Mater. Res. Bull. 20 (1985) 913–919.

[30] Z.M. Sun, D.C. Pan, X.W. Lei, J.G. Mao, J. Solid State Chem. 179 (2006) 3378–3384.

[31] R.A. Gordon, F.J. DiSalvo, R. Pöttgen, J. Alloys Compd. 228 (1995) 16–22.

[32] R. Jardin, V. Babizhetskyy, R. Guérin, J. Bauer, J. Alloys Compd. 353 (2003) 233–239.

[33] B.Ya. Kotur, E.I. Gladyshevskii, Sov. Phys. Crystallogr. 28 (1983) 271 (*In Russian*).

Figure 1. Magnetization as a function of temperature in field of 100 Oe of (a) $Gd_3Co_{3.5}Al_{0.5}$, (b) $Gd_3Co_{3.25}Al_{0.75}$ and (c) $Tb_3Co_{3.25}Al_{0.75}$ (temperature of magnetic transitions from neutron difraction study inserted into **Figure c**).

Figure 2. Magnetization vs temperature of (a) $Gd_3Co_{3.5}Al_{0.5}$ in field of 10 kOe, (b) $Gd_3Co_{3.25}Al_{0.75}$ and (c) $Tb_3Co_{3.25}Al_{0.75}$ in field of 5 kOe (paramagnetic susceptibily vs temperature inserted into **Figures**).

Figure 3. Magnetization vs magnetic field from -140 kOe to 140 kOe of (a) $Gd_3Co_{3.25}Al_{0.75}$ at 2 K and $Tb_3Co_{3.25}Al_{0.75}$ at (b) 100 K, (c) 30 K and (d) 2 K

Figure 4. The isothermal magnetic entropy change $-\Delta S_m$, vs temperature for a field changes of 0-50 kOe of (a) $Gd_3Co_{3.25}Al_{0.75}$ and (b) $Tb_3Co_{3.25}Al_{0.75}$ (maximal value of magnetic entropy change $-\Delta S_m^{max}$ at corresponding temperature vs field change inserted into **Figures**).

Figure 5. Neutron diffraction patterns of $Tb_3Co_{3.25}Al_{0.75}$: (a) at 140 K (paramagnetic state), (b) at 53 K (high-temperature magnetic ordering HT), (c) at 1.5 K (low-temperature magnetic ordering LT) and (d) thermal variation of some reflections. The first and second rows of ticks refer to the nuclear Bragg peaks and magnetic reflections of $Tb_3Co_{3.25}Al_{0.75}$, respectively in **Figures a-c**. Only magnetic

reflections are marked in **Figure b**. The strongest magnetic reflections of low-temperature magnetic ordering are marked in **Figure c**.

Figure 6. Image of magnetic structure of $Tb_3Co_{3.25}Al_{0.75}$ (a) between ~137 K and 38 K and (b) below 38 K (projection on the *bc* plane), The shortest Tb1-2Tb1, Tb1-1Tb2 and Tb1-2Tb2 distances are shown in **Figures** (see **Table 2**).

Figure 7. Thermal evolution of magnetic moments of (a) Tb1, (b) Co2, (c) Tb2 and (d) Co2 sublattices and (e) relative cell parameters of $Tb_3Co_{3.25}Al_{0.75}$.

Figure 8. Relative cell parameters of (a) '$Tb_3Co_{2.2}Si_{1.8}$ [3, 6] - $Tb_3Co_{3.25}Al_{0.75}$ - Tb_3Co_3Ga [4]' row and (b) '$Gd_3Co_{3.5}Al_{0.5}$ - $Gd_3Co_{3.25}Al_{0.75}$' and '$Tb_3Co_{3.25}Al_{0.75}$ - Tb_3Co_3Al' rows.

Table 1.

Unit cell data of the W_3CoB_3-type $R_3Co_{4-x}Al_x$ (x = 1...0.5, *R* = Y, Gd - Ho) compounds, space group *Cmcm*, N 63, *oC*28. The unit cell data of {Gd - Dy}$_3Co_{2.2}Si_{1.8}$ [5, 8] and {Gd, Tb}$_3Co_3Ga$ [6] are given for comparison.

Compound	***a*** (nm)	***b*** (nm)	***c*** (nm)	***V*** (nm^3)	**d** (g/cm^3)	$\mathbf{R_F}$ (%)	**Refs.**
$Y_3Co_{3.25}Al_{0.75}$	0.40910(6)	1.01726(18)	1.29336(24)	0.53825	5.9047	5.5	[a-]
$Gd_3Co_{3.5}Al_{0.5}$ [b-, c-]	0.41093(1)	1.02026(2)	1.30794(3)	0.54836	8.3760	2.5	[a-]
$Gd_3Co_{3.25}Al_{0.75}$	0.41124(3)	1.01897(8)	1.30789(11)	0.54806	8.2838	6.3	[a-]
$Tb_3Co_{3.25}Al_{0.75}$ [d-]	0.40895(3)	1.01301(5)	1.29909(7)	0.53817	8.4980	4.1	[a-]
Tb_3Co_3Al	0.40998(3)	1.01199(9)	1.30349(12)	0.54081	8.3584	6.5	[a-]
$Dy_3Co_{3.25}Al_{0.75}$	0.40790(2)	1.00837(6)	1.29593(8)	0.53303	8.7136	4.9	[a-]
$Ho_3Co_{3.25}Al_{0.75}$	0.40705(3)	1.00514(8)	1.29352(11)	0.52923	8.8676	4.8	[a-]
$Gd_3Co_{2.2}Si_{1.8}$	0.41229	1.0308	1.2793	0.54369	7.9648		[5]
$Tb_3Co_{2.2}Si_{1.8}$	**0.40967**	1.02439	1.27102	0.53340	8.1810		[8]
$Dy_3Co_{2.2}Si_{1.8}$	**0.40828**	1.01898	1.26913	0.52800	8.3997		[8]
Gd_3Co_3Ga	0.4119	1.0080	1.3140	0.54557	8.7448		[6]
Tb_3Co_3Ga	0.4109	1.0070	1.3070	0.54081	8.8835		[6]

[a-] this work;

[b-] Crystallographic data used with permission of JCPDS - International Centre for Diffraction Data;

[c-] $Gd_3Co_{3.5}Al_{0.5}$: Gd1 8*f* [0, 0.2872(2), 0.6049(2)], Gd2 4*c* [0, 0.0064(1), 1/4], Co1 8*f* [0, 0.4276(3), 0.0884(2)], Co2 4*c* [0, 0.3020(6), 1/4], M = $Co_{0.5}Al_{0.5}$ 4*a* [0, 0, 0], atomic displacement parameters of all atoms β_{11} = 0.014805, β_{22} = 0.002402, β_{33} = 0.001461 ($\beta_{11} = B_{11}/[2a]^2$, $\beta_{22} = B_{11}/[2b]^2$, $\beta_{33} = B_{33}/[2c]^2$);

[d-] $Tb_3Co_{3.25}Al_{0.75}$: Tb1 (8*f*) [0, 0.2863(3), 0.6047(2)], Tb2 (4*c*) [0, 0.0025(5), 1/4], Co1 (8*f*) [0, 0.4246(7), 0.0902(5)], Co2 (4*c*) [0, 0.3019(11), 1/4], M (4*a*) [0, 0, 0], M = $Co_{0.25}Al_{0.75}$, atomic displacement parameters of all atoms β_{11} = 0.014949, β_{22} = 0.002436, β_{33} = 0.001481 ($\beta_{11} = B_{11}/[2a]^2$, $\beta_{22} = B_{11}/[2b]^2$, $\beta_{33} = B_{33}/[2c]^2$).

Table 2. Interatomic distances of W_3CoB_3-type $Tb_3Co_{3.25}Al_{0.75}$ (ESD ±0.0004): space group *Cmcm*, N 63, *a* = 0.40895(2) nm, *b* = 1.01301(5) nm, *c* = 1.29909(7) nm, *Z* = 4, Tb1 (8*f*) [0, 0.2863(3), 0.6047(2)], Tb2 (4*c*) [0, 0.0025(5), 1/4], Co1 (8*f*) [0, 0.4246(7), 0.0902(5)], Co2 (4*c*) [0, 0.3019(11), 1/4], M (4*a*) [0, 0, 0], M = $Co_{0.25}Al_{0.75}$, R_F = 4.1 %.[a-] In the Table are given the ratio of interatomic distances to the sum of the atomic radii of the corresponding atoms Δ (r_{Tb} = 0.17788 nm, r_{Co} = 0.1251 nm, r_{Al} = 0.14317 nm and for M atom the $r_M = 0.25 \cdot r_{Co} + 0.75 \cdot r_{Al}$) [19, 20] $\Delta = D/(R_{atom1} + R_{atom2})$ and coordination numbers **CN**. The shortest Tb-Tb, Tb-Co and Co-Co distances are selected by a boldface character.

Atom -Atom	D (nm)	Δ	Atom -Atom	D (nm)	Δ
Tb1 - **1Co1**	**0.28937**	**0.96**	Co1 - **1Co2**	**0.24196**	**0.97**
2Co2	**0.29227**	**0.96**	2M	0.24774	0.94
1Co1	0.29347	0.97	1Co1	0.27975	1.12
2Co1	0.29633	0.98	**1Tb1**	**0.28937**	**0.96**
1M	0.32033	1.01	1Tb1	0.29347	0.97
2M	0.32737	1.03	2Tb1	0.29633	0.98
2Tb1	**0.34816**	**0.98**	2Tb2	0.30188	1.00
1Tb2	**0.34817**	**0.98**	**CN = 10**		
2Tb2	0.35102	0.99			
1Tb1	0.37752	1.06	Co2 - **2Co1**	**0.24196**	**0.97**
CN = 15			**2Tb2**	**0.28828**	**0.95**
			4Tb1	**0.29227**	**0.96**
Tb2 - **2Co2**	**0.28828**	**0.95**	1Tb2	0.30330	1.00
4Co1	0.30188	1.00	**CN = 9**		
1Co2	0.30330	1.00	M - 4Co1	0.24774	0.94
2M	0.32478	1.03	2Tb1	0.32033	1.01
2Tb1	**0.34817**	**0.98**	2Tb2	0.32478	1.03
4Tb1	0.35102	0.99	4Tb1	0.32737	1.03
CN = 15			**δ = 12**		

Table 3.

Magnetic properties of W_3CoB_3-type {Gd - Ho}$_3Co_{3.25}Al_{0.75}$ and $Gd_3Co_{3.5}Al_{0.5}$ compounds: effective magnetic moment per formula unit (M_{eff}/fu) and per Co (M_{eff}/Co) (assuming that rare earths take the theoretical effective moment values [21]), paramagnetic Weiss temperature (Θ_P), Curie point (T_C), temperature of spin reorientation transition (T_{SR}), magnetization per formula unit in field of 140 kOe (M_{140kOe}/fu), remanent magnetisation per formula unit (M_{res}/fu), coercive field (H_{coer}), critical field (H_{crit}) and magnetocaloric effect (MCE) in terms of isothermal magnetic entropy change, ΔS_m, for a field change of 0-50 kOe and 0-140 kOe. Magnetic properties of $Tb_3Co_{2.2}Si_{1.8}$ [8] are given for comparison.

Compound	M_{eff}/fu (μ_B)	M_{eff}/Co (μ_B)	Θ_P (K)	$T_{C,N}$	M_{140kOe}/fu (μ_B)	M_{res}/fu (μ_B)	H_{coer} (kOe)	H_{crit} (kOe)	ΔS_m (J/kg·K) (0-50kOe)	ΔS_m (J/kg·K) (0-140kOe)
$Gd_3Co_{3.5}Al_{0.5}$	14.1	1.7	198	T_C = 196 K						
$Gd_3Co_{3.25}Al_{0.75}$	14.0	1.5	39	T_C = 161 K	19.8 (2 K)	- (2 K)	- (2 K)	- (2 K)	-4.9 (135-145 K)	-11.3 (125-145 K)
$Tb_3Co_{3.25}Al_{0.75}$	17.1	1.7	118	T_C = 151 K T_{SR} ~ 42 K	15.2 (100 K) 18.2 (30 K) 17.3 (2 K)	- 9.1 (30 K) 9.7 (2 K)	- 14 (30 K) 15 (2 K)	- ~10 (30 K) ~12 (2 K)	-3.7 (115-135 K) +13.6 (10 K)	-9.9 (115-135 K) +32.9 (5 K)
$Dy_3Co_{3.25}Al_{0.75}$				T_C~100 K[a-] T_{SR}~30 K[a-]						
$Ho_3Co_{3.25}Al_{0.75}$				T_C ~65 K[a-] T_{SR}~20 K[a-]						
$Tb_3Co_{2.2}Si_{1.8}$[b-] [8]	17.0	1.6	118	T_C = 132 K T_{SR} = 42 K	16.5[c-] (75 K) 18.0[c-] (2 K)	- 12.3[c-] (2 K)	- 17 (2 K)	- 30 (2 K)		

[a-] tentative from de Gennes rule [21];

[b-] At ~127 K - 53 K ferro-antiferromagnet: $(\mathbf{F}_b + \mathbf{AF}_c)^{\mathbf{K0}}$ **Cmc′m** + canted spiral $\mathbf{AF}_{\mathbf{MK0(Tbji)}}{}^{\mathbf{K1}}$, at 53-43 K ferro-antiferromagnet $(\mathbf{AF}_b + \mathbf{F}_b + \mathbf{AF}_c + \mathbf{F}_c)^{\mathbf{K0}}$ **C2′/m** + canted spiral $\mathbf{AF}_{\mathbf{MK0(Tbji)}}{}^{\mathbf{K1}}$ and below 43 K ferro-antiferromagnet $(\mathbf{AF}_b + \mathbf{F}_c)^{\mathbf{K0}}$ **Cmcm′** + canted spiral $\mathbf{AF}_{\mathbf{MK0(Tbji)}}{}^{\mathbf{K1}}$ ($\mathbf{K}_0$ = [0, 0, 0] and $\mathbf{K}_1$ = [±K_x, 0, 0] ($K_x \approx 3/10$) [8];

[c-] in field of 70 kOe

Table 4.

Coordinates of the 8*f* sites for Tb1, Co1 and 4*c* sites for Tb2 and Co2 in the *Cmcm* space group (*Cmcm* = {**1**, $\mathbf{m}_x$} × {**1**, $\mathbf{m}_y$/[0, 0, 1/2]} × {**1**, **i**} × {**1**, **1**/[1/2, 1/2, 0]} retained by $Tb_3Co_{3.25}Al_{0.75}$. The corresponding symmetry operators of the unit cell and magnetic unit cell with $\mathbf{K}_0$ = [0, 0, 0] wave vector and magnetic space group are given for the high-temperature HT and low-temperature LT magnetic orders. The $\mathbf{M}_a$. $\mathbf{M}_b$ and $\mathbf{M}_c$ are *a*-, *b*- and *c*-axis commensurate magnetic component of corresponding Tbj^i atoms and $\mathbf{m}_a$. $\mathbf{m}_b$ and $\mathbf{m}_c$ are *a*-, *b*- and *c*-axis commensurate magnetic component of corresponding Coj^i atoms.

.**a)**. high-temperature HT magnetic order of **Cmc′m** magnetic space group (N 63.4.514) [18]: **Cmc′m** = {**1**, $\mathbf{m}_x$} × {**1**, $\mathbf{m}_z$/[0, 0, 1/2]} × {**1**, **i′**} × {**1**, **1**/[1/2, 1/2, 0]}.

N	x/*a*	y/*b*	z/*c*	Symmetry operator of unit cell	M_a	M_b	M_c	m_a	m_b	m_c	Symmetry operator of magnetic cell
$Tb1^1$, $Co1^1$	0	$+y_1$	$+z_1$	**1, m**$_x$	0	+	+	0	-	-	**1, m**$_x$
$Tb1^2$, $Co1^2$	0	$-y_1$	$1/2+z_1$	**m**$_y$/[0, 0, 1/2], **2**$_z$/[0, 0, 1/2]	0	+	-	0	-	+	**m**$_y$′/[0,0,1/2], **2**$_z$′/[0,0,1/2]
$Tb1^3$, $Co1^3$	0	$-y_1$	$-z_1$	**i, 2**$_x$	0	+	+	0	-	-	**i′, 2**$_x$′
$Tb1^4$, $Co1^4$	0	$+y_1$	$1/2-z_1$	**2**$_y$/[0, 0, 1/2], **m**$_z$/[0, 0, 1/2]	0	+	-	0	-	+	**2**$_y$/[0,0,1/2], **m**$_z$/[0,0,1/2]
$Tb1^5$, $Co1^5$	1/2	$1/2+y_1$	$+z_1$	**1**/[1/2, 1/2, 0], **m**$_x$/[1/2, 1/2, 0]	0	+	+	0	-	-	**1**/[1/2,1/2,0], **m**$_x$/[1/2,1/2,0]
$Tb1^6$, $Co1^6$	1/2	$1/2-y_1$	$1/2+z_1$	**m**$_y$/[1/2,1/2,1/2], **2**$_z$/[1/2,1/2,1/2]	0	+	-	0	-	+	**m**$_y$′/[1/2,1/2,1/2], **2**$_z$′/[1/2,1/2,1/2]
$Tb1^7$, $Co1^7$	1/2	$1/2-y_1$	$-z_1$	**i**/[1/2, 1/2, 0], **2**$_x$/[1/2, 1/2, 0]	0	+	+	0	-	-	**i′**/[1/2, 1/2, 0], **2**$_x$′/[1/2, 1/2, 0]
$Tb1^8$, $Co1^8$	1/2	$1/2+y_1$	$1/2-z_1$	**2**$_y$/[1/2,1/2,1/2], **m**$_z$/[1/2,1/2,1/2]	0	+	-	0	-	+	**2**$_y$/[1/2,1/2,1/2], **m**$_z$/[1/2,1/2,1/2]
$Tb2^1$, $Co2^1$	0	$+y_2$	1/4	**1, m**$_x$, **2**$_y$/[0, 0, 1/2], **m**$_z$/[0, 0, 1/2]	0	+	0	0	-	0	{**1, m**$_x$, **2**$_y$/[0,0,1/2], **m**$_z$/[0,0,1/2]}
$Tb2^2$, $Co2^2$	0	$-y_2$	3/4	**m**$_y$/[0, 0, 1/2], **2**$_z$/[0, 0, 1/2], **i, 2**$_x$	0	+	0	0	-	0	**m**$_y$′/[0,0,1/2], **2**$_z$′/[0,0,1/2], **i′, 2**$_x$′

$Tb2^3$, $Co2^3$	1/2	1/2+y_2	1/4	**1**/[1/2, 1/2, 0], $\mathbf{m}_x$/[1/2, 1/2, 0], $\mathbf{2}_y$/[1/2,1/2,1/2], $\mathbf{m}_z$/[1/2,1/2,1/2]	0	+	0	0	-	0	**1**/[1/2, 1/2, 0], $\mathbf{m}_x$/[1/2, 1/2, 0], $\mathbf{2}_y$/[1/2,1/2,1/2], $\mathbf{m}_z$/[1/2,1/2,1/2]
$Tb2^4$, $Co2^4$	1/2	1/2-y_2	3/4	$\mathbf{m}_y$/[1/2,1/2,1/2], $\mathbf{2}_z$/[1/2,1/2,1/2], **i**/[1/2, 1/2, 0], $\mathbf{2}_x$/[1/2, 1/2, 0]	0	+	0	0	-	0	$\mathbf{m}_y'$/[1/2,1/2,1/2], $\mathbf{2}_z'$/[1/2,1/2,1/2], **i′**/[1/2, 1/2, 0], $\mathbf{2}_x'$/[1/2, 1/2, 0]

b). low-temperature LT magnetic order of **C2′/c** magnetic space group (N 15.3.94) [18]: **C2′/c** = {**1**, $\mathbf{m}_z$/[0, 0, 1/2]} × {**1**, **i′**} × {**1**, **1**/[1/2, 1/2, 0]}.

N	x/*a*	y/*b*	z/*c*	Symmetry operator of unit cell	M_a	M_b	M_c	m_a	m_b	m_c	Symmetry operator of magnetic cell
$Tb1^1$, $Co1^1$	0	+y_1	+z_1	**1**, $\mathbf{m}_x$	+	+	+	-	-	-	**1**
$Tb1^2$, $Co1^2$	0	-y_1	1/2+z_1	$\mathbf{m}_y$/[0, 0, 1/2], $\mathbf{2}_z$/[0, 0, 1/2]	+	+	-	-	-	+	$\mathbf{2}_z'$/[0, 0, 1/2]
$Tb1^3$, $Co1^3$	0	-y_1	-z_1	**i**, $\mathbf{2}_x$	+	+	+	-	-	-	**i′**
$Tb1^4$, $Co1^4$	0	+y_1	1/2-z_1	$\mathbf{2}_y$/[0, 0, 1/2], $\mathbf{m}_z$/[0, 0, 1/2]	+	+	-	-	-	+	$\mathbf{m}_z$/[0, 0, 1/2]
$Tb1^5$, $Co1^5$	1/2	1/2+y_1	+z_1	**1**/[1/2, 1/2, 0], $\mathbf{m}_x$/[1/2, 1/2, 0]	+	+	+	-	-	-	**1**/[1/2, 1/2, 0]
$Tb1^6$, $Co1^6$	1/2	1/2-y_1	1/2+z_1	$\mathbf{m}_y$/[1/2, 1/2, 1/2], $\mathbf{2}_z$/[1/2, 1/2, 1/2]	+	+	-	-	-	+	$\mathbf{2}_z'$/[1/2, 1/2, 1/2]
$Tb1^7$, $Co1^7$	1/2	1/2-y_1	-z_1	**i**/[1/2, 1/2, 0], $\mathbf{2}_x$/[1/2, 1/2, 0]	+	+	+	-	-	-	**i′**/[1/2, 1/2, 0]
$Tb1^8$, $Co1^8$	1/2	1/2+y_1	1/2-z_1	$\mathbf{2}_y$/[1/2, 1/2, 1/2], $\mathbf{m}_z$/[1/2, 1/2, 1/2]	+	+	-	-	-	+	$\mathbf{m}_z$/[1/2, 1/2, 1/2]
$Tb2^1$, $Co2^1$	0	+y_2	1/4	**1**, $\mathbf{m}_x$, $\mathbf{2}_y$/[0, 0, 1/2], $\mathbf{m}_z$/[0, 0, 1/2]	+	+	0	-	-	0	{**1**, $\mathbf{m}_z$/[0, 0, 1/2]}
$Tb2^2$, $Co2^2$	0	-y_2	3/4	$\mathbf{m}_y$/[0, 0, 1/2], $\mathbf{2}_z$/[0, 0, 1/2], **i**, $\mathbf{2}_x$	+	+	0	-	-	0	$\mathbf{2}_z'$/[0, 0, 1/2], **i′**
$Tb2^3$, $Co2^3$	1/2	1/2+y_2	1/4	**1**/[1/2, 1/2, 0], $\mathbf{m}_x$/[1/2, 1/2, 0], $\mathbf{2}_y$/[1/2, 1/2, 1/2], $\mathbf{m}_z$/[1/2, 1/2, 1/2]	+	+	0	-	-	0	**1**/[1/2, 1/2, 0], $\mathbf{m}_z$/[1/2, 1/2, 1/2]
$Tb2^4$, $Co2^4$	1/2	1/2-y_2	3/4	$\mathbf{m}_y$/[1/2, 1/2, 1/2], $\mathbf{2}_z$/[1/2, 1/2, 1/2], **i**/[1/2, 1/2, 0], $\mathbf{2}_x$/[1/2, 1/2, 0]	+	+	0	-	-	0	$\mathbf{2}_z'$/[1/2, 1/2, 1/2], **i′**/[1/2, 1/2, 0]

Table 5.

Unit cell data and magnetic parameters of the W_3CoB_3-type $Tb_3Co_{3.25}Al_{0.75}$ compound at different temperatures: unit cell data, magnetic moment $\mathbf{M}_a^{K0}$, $\mathbf{M}_b^{K0}$ and $\mathbf{M}_c^{K0}$ along *a, b* and *c* axis, respectively of corresponding Tbj^i and Coj^i atoms and resulting magnitude magnetic moment $|\mathbf{M}|^{K0}$ of the corresponding atom with the wave vectors $\mathbf{K}_0$ = [0, 0, 0]. R_F (crystal structure) and R_F^m (magnetic structure) are reliability factors.

T (K)	Unit cell data	R_F (%)	Atom	$\mathbf{M}_a^{K0}$ (μ_B)	$\mathbf{M}_b^{K0}$ (μ_B)	$\mathbf{M}_c^{K0}$ (μ_B)	$\lvert\mathbf{M}\rvert^{K0}$ (μ_B)	R_F^m (%)
			Paramagnet					
298[a-]	*a* = 0.40895(2) nm *b* = 1.01301(5) nm *c* = 1.29909(7) nm	4.1						
140	*a* = 0.40791(9) nm *b* = 1.0099(2) *c* = 1.2954(3) nm	8.6						
			T_C^{ND} ~130 K: *b*-Ferromagnet and *c*-Antiferromagnet					
			$(\mathbf{F}_b + \mathbf{AF}_c)^{K0}$ of **Cmc′m** magnetic space group ($\mathbf{K}_0$ = [0, 0, 0])					
53	*a* = 0.40751(5) nm	3.6	$Tb1^1$, $Tb1^3$, $Tb1^5$, $Tb1^7$	0	+7.8(1)	-4.02(7)	8.7(1)	3.3
	b = 1.00979(14) nm		$Tb1^2$, $Tb1^4$, $Tb1^6$, $Tb1^8$	0	+7.8(1)	+4.02(7)	8.7(1)	
	c = 1.29425(14) nm		$Tb2^1$, $Tb2^3$, $Tb2^2$, $Tb2^4$	0	5.5(1)	0	5.5(1)	
			$Co1^1$, $Co1^3$, $Co1^5$, $Co1^7$	0	-0.35(5)	-0.18(5)	0.28(5)	
			$Co1^2$, $Co1^4$, $Co1^6$, $Co1^8$	0	-0.35(5)	+0.18(5)	0.39(5)	
			$Co2^1$, $Co2^3$, $Co2^2$, $Co2^4$	0	-0.18(5)	0	0.18(5)	
			T_{SR}^{ND} ~ 38 K: *ab*-Ferromagnet and *c*-Antiferromagnet					
			$(\mathbf{F}_a + \mathbf{F}_b + \mathbf{AF}_c)^{K0}$ of **C2′/c** magnetic space group ($\mathbf{K}_0$ = [0, 0, 0])					
1.5	*a* = 0.40740(4) nm	3.6	$Tb1^1$, $Tb1^3$, $Tb1^5$, $Tb1^7$	1.05(8)	8.0(1)	-4.08(9)	9.0(1)	3.0

b = 1.00891(12) nm	$Tb1^2$, $Tb1^4$, $Tb1^6$, $Tb1^8$	1.05(8)	8.0(1)	4.08(9)	9.0(1)
c = 1.29425(14) nm	$Tb2^1$, $Tb2^3$, $Tb2^2$, $Tb2^4$	6.3(1)	5.7(1)	0	8.5(1)
	$Co1^1$, $Co1^3$, $Co1^5$, $Co1^7$	-0.41(5)	-0.37(4)	-0.28(3)	0.62(7)
	$Co1^2$, $Co1^4$, $Co1^6$, $Co1^8$	-0.41(5)	-0.37(4)	+0.28(3)	0.62(7)
	$Co2^1$, $Co2^3$, $Co2^2$, $Co2^4$	-0.21(4)	-0.19(3)	0	0.28(5)

[a]-X-ray powder data

Highlights

>{Y,Gd - Ho}$_3$Co$_{4-x}$Al$_x$ (x = 0.5-1) crystallize in the W_3CoB_3-type structure.

>$Gd_3Co_{3.25}Al_{0.75}$ and $Tb_3Co_{3.25}Al_{0.75}$ show ferrimagnetic ordering at 161 K and 151 K.

>$Gd_3Co_{3.25}Al_{0.75}$ and $Tb_3Co_{3.25}Al_{0.75}$ are soft ferrimagnets below ferrimagnetic ordering.

>$Tb_3Co_{3.25}Al_{0.75}$ is hard ferrimagnet below low-temperature transition at 42 K.

>$Tb_3Co_{3.25}Al_{0.75}$ is complex ferrimagnet with **Cmc′m** and **C2′/c** magnetic space groups.

W_3CoB_3-type $Tb_3Co_{3.25}Al_{0.75}$

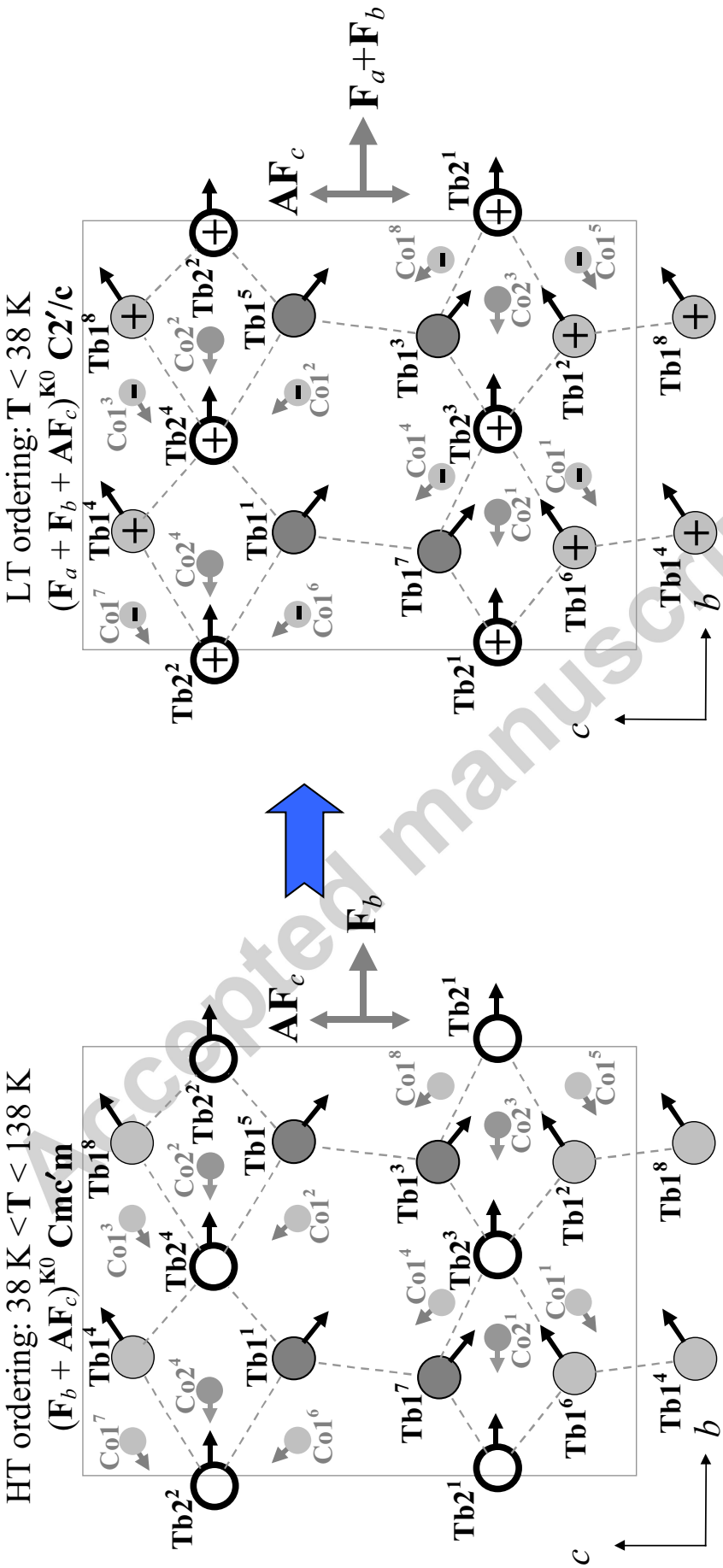

New {Y, Gd - Ho}$_3$Co$_{3.25}$Al$_{0.75}$, Gd$_3$Co$_{3.5}$Al$_{0.5}$ and Tb$_3$Co$_3$Al compounds crystallize in the W_3CoB_3-type structure (*Cmcm*. N 63, *oC*28). Gd$_3$Co$_{0.5}$Al$_{0.5}$, Gd$_3$Co$_{3.25}$Al$_{0.75}$ and Tb$_3$Co$_{3.25}$Al$_{0.75}$ exhibit ferrimagnetic ordering below 196 K, 161 K and 151 K, respectively. Tb$_3$Co$_{3.25}$Al$_{0.75}$ shows a spin-reorientation transition at ~42 K. Below the ferrimagnetic ordering temperature Gd$_3$Co$_{3.25}$Al$_{0.75}$ and Tb$_3$Co$_{3.25}$Al$_{0.75}$ are soft ferrimagnets, meanwhile Tb$_3$Co$_{3.25}$Al$_{0.75}$ shows magnetic hardness below the spin-reorientation transition with remanent magnetization per formula unit of 9.7 μ_B and coercive field of 15 kOe at 2 K.

The magnetocaloric effects (isothermal magnetic entropy change) of Gd$_3$Co$_{3.25}$Al$_{0.75}$ and Tb$_3$Co$_{3.25}$Al$_{0.75}$ reach maximum values of -4.9 J/kg·K at 135-145 K and -3.7 J/kg·K at 115-135 K, respectively, for a field change of 0-50 kOe. Low temperature magnetic ordering in Tb$_3$Co$_{3.25}$Al$_{0.75}$ is accompanied by a positive magnetocaloric effect of +13.6 J/kg·K at 10 K for a field change of 0-50 kOe and +0.9 J/kg·K at 45 K for a field change of 0-10 kOe.

Neutron diffraction study in zero applied field shows mixed ferro-antiferromagnetic ordering of Tb$_3$Co$_{3.25}$Al$_{0.75}$ with a wave vector $\mathbf{K}_0$ = [0, 0, 0]. Below ~ 137 K Tb$_3$Co$_{3.25}$Al$_{0.75}$ exhibits non-collinear ferrimagnetic ordering of terbium and cobalt sublattices with resulting of *b*-axis ferromagnetic and *c*-axis antiferromagnetic components of **Cmc′m** = {**1**, $\mathbf{m}_x$} × {**1**, $\mathbf{m}_z$/[0, 0, 1/2]} × {**1**, **i′**} × {**1**, **1**/[1/2, 1/2, 0]} magnetic space group. The spin-reorientation transition in Tb$_3$Co$_{3.25}$Al$_{0.75}$ below ~38 K corresponds to appearance of additional *a*-axis ferromagnetic component and decreasing of symmetry of magnetic ordering down to **C2′/c** = {**1**, $\mathbf{m}_z$/[0, 0, 1/2]} × {**1**, **i′**} × {**1**, **1**/[1/2, 1/2, 0]} magnetic space group.